Article:
Cai, N, Xia, S, Li, X et al. (7 more authors) (2021) Influence of the ratio of Fe/Al2O3 on waste polypropylene pyrolysis for high value-added products. Journal of Cleaner Production, 315. 128240. ISSN 0959-6526

https://doi.org/10.1016/j.jclepro.2021.128240

Influence of the ratio of Fe/Al_2O_3 on waste polypropylene pyrolysis for high value-added products

Ning Cai[1], Sunwen Xia[1], Xiaoqiang Li[1], Lin Sun[1],Pietro Bartocci[2], Francesco Fantozzi[2],Haozhe Zhang[3],Hanping Chen[1], Paul T. Williams[4], Haiping Yang[1]*

[1]*State Key Laboratory of Coal Combustion, School of Energy and Power Engineering, Huazhong University of Science and Technology, Wuhan, 430074, PR China*

[2]*Department of Engineering, University of Perugia, via G. Duranti 67, 06125, Perugia, Italy*

[3]*Institution of Resource & Environment, Henan Polytechnic University,Jiaozuo, 454150,PR China*

[4]*School of Chemical and Process Engineering, University of Leeds, Leeds, LS2 9JT UK*

Abstract: Thermo conversion technology has been considering as a promising one to realize the high value of waste plastics. However, low selectivity of target products limited the further utilizationfundamentally. Herein, alumina supported with different iron ratio catalyst was introduced to improve the properties of products. The results show that the hydrogen in gaseous product increased dramatically with the increase in the iron ratio, and the maximum content was 82 vol.% while the ratio of iron and alumina was 2:1. For liquid oil, the yield suffered from an apparent reduction, while the content of naphthalene increased first and then decreased and reached the maximum of over 70 area% when the iron and alumina was 1:2. Simultaneously,

carbon deposits yield on catalysts increased with the increase ironratio, and the maximum one of approximately 42 wt.% was obtained fromthe catalyst with ratio of 1:1. Further research shows that the carbon deposits on the catalyst were composed of abundant carbon nanotubes (CNTs), varying from ~8 to 20 nm of diameters.This study presents a feasible strategy to deal with plastics.

Keywords: Waste plastics; Iron catalysts;catalytic-pyrolysis; Carbon nanotubes; Hydrogen

1. Introduction

A recent analysis showed that a worldwide cumulative total of approximately 8,300 million tonnes of plastic waste was generated as of2017,and approximately 60% of the waste was landfilled or discarded(Geyer, 2017). Furthermore, as COVID-19 has become a global issue since the beginning of 2020, personal protective equipment (PPE), usually made of plastic,has become essential to prevent infections.It was estimated that approximately 129 billion face masks and 65 billion glovesare being consumed monthly, which means that hundreds of millions of tonnes of plastic wastearebeing produced(Prata, 2020). Traditional disposalapproaches like landfilling not only causes pollution to the natural environment but leads to the spread of the virus.In order to avoid the virus's spread, some essentialpre-treatments like uperization should be introduced before landfilling process. Thisis not an economically viable solution for such large quantities of waste.

Thermal chemical conversion is considered to be an economically profitable

approachto the utilisation of waste plastics (Miandad, 2017). It has been reported that fast pyrolysis and gasification have total NPVs of $149MM and $96MM, respectively(Bora, 2020), let alone catalytic pyrolysis where more valuable productssuch as hydrogen (H_2) and carbon nanotubes (CNTs) could be gathered(Faisal, 2014).Barbarias et al.(Barbarias, 2018) found that the introduction of a catalyst can dramatically promote H_2 production.Similar resultswere obtained from Wu et al.(Wu, 2010), who demonstrated a higher H_2yield in the presence of a catalyst.The production of liquid products was also explored during the catalytic pyrolysis process.López et al.(López, 2011) found that liquid products produced from the pyrolysis of waste plastics contain lower molecular weight aromatic hydrocarbons.Williams(Williams, 2020)concluded that many carbon deposits, i.e. CNTs, are produced in the presence of transition metal catalysts.

Apparently, the physical and chemical properties of the catalysts play an important rolein the catalytic process. Li et al. (Li, 2017)found that catalysts with a high BET surface area and uniformly dispersed iron oxide particles exhibit a better catalytic activity in terms of H_2 yield.Abdul-Wahab et al.(Abdul-Wahab, 2013)obtained optimisedhydrogenation results with a smaller and better dispersion of catalyst metal particles. However,Chen et al. (Chen, 2005)found that a smaller crystal size results in a higher saturation concentration of carbon, leadingto fast deactivation and a lower final carbon yield.In addition, Janardhan et al. (Janardhan, 2014)found that a lower pore volume of the catalyst decreases the activity of the catalyst, and Jia et al.(Jia, 2020)reported that moderate metal-support interactions lead to optimal

CNTs.Moreover, Yao et al. (Yao, 2020b)proved that bimetallic catalysts exhibit higher yields of hydrogen and carbon deposits.All of these results proved that the catalysttype or properties play an essential role in the process of plastic recycling.

Iron-based catalysts have been widely used in thermal conversion processes because of their lowcost and high efficiency(Ramadhani, 2020), and Al_2O_3 has been extensively used as a support materialowing to its competitive price, excellent mechanical strength, and thermal stability(Yao, 2020b).For example, Jin et al. (Jin, 2013) reported thatFe/Al_2O_3catalystleadsto a higher yield of hydrogenfor catalytic methane decomposition. In addition, Xu et al.(Xu, 2014)obtained similar results, showing thatFe/Al_2O_3 catalystsexhibit better effects on theoxidative dehydrogenation of ethane.Moreover, Fe-Alcatalysts have also been used inthe thermal conversion of waste plastics, and preferable H_2yields and/or carbon production were obtained fromYao(Yao, 2020a).Although there have been significant effortsmade in waste plastic recycling, most studies haveconcentrated on parts oftheproducts, such as syngas(Kumagai, 2017) and liquid fuel(Rodriguez, 2019),the co-production of syngasand char(Veses, 2020)or H_2 and carbon nanotubes (Williams, 2020).However, the relationship of the ratio of Fe/Al_2O_3 with plastics pyrolysis behavior and product is not clear. Therefore, building the relationship of catalyst composition with product characteristics and revealing the catalytic mechanism of waste plastics are of great significance for the efficient pyrolysis and high-quality utilization of waste plastic.

Herein, various ratios of iron catalysts were introduced to further study the catalytic pyrolysis properties of PP, and the catalytic process and the physicochemical

properties of products for different situations were analyzed in detail. Furthermore, the relationship between the product features and iron ratio was discussed, and the possible reaction mechanism was explored in depth. It is significant for catalyst design and plastics wastes pyrolysis.

2. Experimental methods

2.1 Materials and catalyst

The raw plastic waste material used in this study was waste PP collectedfrom disposable lunch boxes. Proximate and ultimate analyses are presented in **Table 1**.The proximate analysis showed that the materials used contained abundant volatile matter, up to nearly 100 wt.%. Carbon and hydrogen comprise approximately 99 wt.% of the polypropylene according to the ultimate analysis.

Table 1

Proximate and ultimate analysesof the polypropylene

Sample	Proximate analysis (wt.%)$_{ar}$				Ultimate analysis (wt.%)$_{db}$			
	M	Ash	V	FC	C	H	S	O*
Polypropylene	0.04	0.06	99.87	0.03	85.18	13.74	0.17	0.86

M, moisture; V, volatiles; FC, fixed carbon;

ar, as received; db, dry based.

*Calculated by difference

Iron nitrate nonahydrate($Fe(NO_3)_3 9H_2O$, ≥98.50%) and nanometre-sized(10 nm) aluminium oxide (Al_2O_3, ≥99.99%) were purchased from Sigma Aldrich (China).

Absolute ethanol (≥99.70%) was purchased from Sinopharm Chemical Reagent Co., Ltd. (China). All chemicals were of analytical grade.

Fe/Al_2O_3catalysts were prepared using the impregnation method.Typically, for the preparation ofa Fe/Al_2O_3 catalyst with a mass ratio of Fe to Al_2O_3 of1:10, 7.21 g of $Fe(NO_3)_3·9H_2O$ was placed inethyl alcohol(50 mL)and stirred for 30 min at 25 °C, and when the $Fe(NO_3)_3$ was completely dissolved, 10.00 g ofAl_2O_3 was introducedand used as the substrate material.The mixed solution was stirred for several hoursat 50 °Cwith a thermostaticmagnetic stirrer until the solution became a slurry. The slurry was then dried at105 °Cin a thermostatically controlledoven for12 h, and the dried solid was ball milled to produce particles smaller than 0.08 mm.Later, the prepared material was calcined at 800 °C under an air atmosphere at a heating rate of 10 °C $min^{-1}$and held at 800 °C for 2 h. The obtained catalyst sample was designated as $Fe1Al_2O_310$. The other Fe-basedAl_2O_3catalysts with different ratios were prepared using the same method with an altered Fe and Al_2O_3 input.The catalysts prepared were designated as$Fe1Al_2O_320$, $Fe1Al_2O_310$, $Fe1Al_2O_35$, $Fe1Al_2O_32$,$Fe1Al_2O_31$, and$Fe2Al_2O_31$, with Fe:alumina ratios of 1:20, 1:10, 1:5, 1:1, and 2:1,respectively. Notably, only ferric species and aluminium oxide were left after the complete evaporation of alcohol, and there was no loss during thepreparation process. Therefore, the practical ratio of Fe in the as-obtained catalysts should be the same as the pre-set value.Simultaneously, to avoid the influence of heat and mass transfer, pure aluminium oxide was used as a control group to show the influence of the Feintroduction. Notably, the catalyst was not reduced prior to its utilization

2.2 Catalytic-pyrolysis experimental system

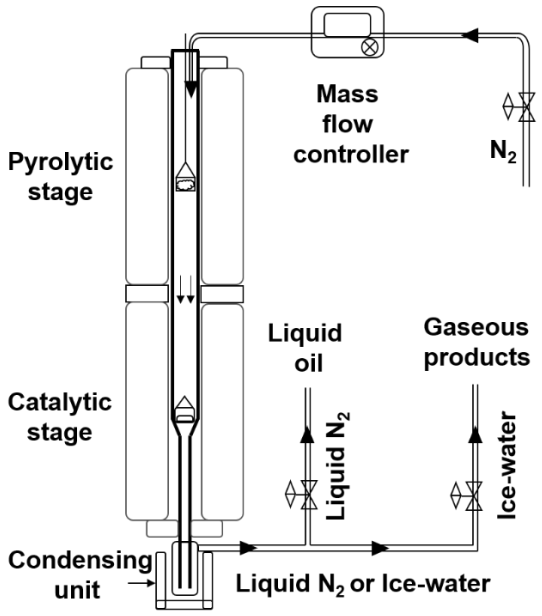

Figure 1. Schematic diagram ofcatalytic-pyrolysis system.

Thecatalyticpyrolysis experiments were carried out in a two-stage fixed-bed reactor, as shown in Figure 1.Upper stage and lower stage of the reactor are corresponding to the pyrolytic stage and catalytic stage, respectively. After condensation, liquid oil or gaseous products was collected with liquid N_2 and ice-waste separately.For each trial,acatalyst (0.5 g) was placed into a quartz catalyst holder in the lower catalyst stage of the reactor. Nitrogen was introduced into the reactor at a flow rate of 500 $mLmin^{-1}$for 30 min to purge the reactor and producean inert atmosphere, followed by agas flow rate of 100 $mLmin^{-1}$,which was used throughout the experiment. The lower catalytic stage was preheated to 800 °Cat a heating rate of 20 °C min^{-1}. Once the catalyst stage temperature had stabilised, a1 g plastic sample (ground particles of 1–2 mm)held in a quartz holder was introduced into the middle of the upper pyrolytic stage and heated at a rate of 10 °C $min^{-1}$to 500 °C and kept isothermal for 10 min.The

reaction time for each pyrolysis catalysis experiment was set to 30 min.

Liquid oil and gaseous products were collected separately using separate repeated experiments. Liquid oil was cooled and collected with liquid nitrogen, andthegaseous products were collected usingan ice water condensing system. The carbonaceous solid deposited onto the catalysts in the lower quartz holder was collected at the end of the experiment. The gas yieldwas determined by combining the total gas volume, gas density, and gas volume determined by a mass flow controller(Chen, 2018). The yields of the solid and liquid products were calculated using Eqs. (1) and (2), respectively. In addition, the hydrogen yield and efficiency were evaluated using Eqs. (3) and (4), respectively.Each experiment was carried out at least three times, and the average data werecalculated fromthree sets of data with an error of less than 5%.However, part of the visible yellow liquid oil adhered to the inner wall of the reactor, which have difficulty to collect, leading to a partial loss of quality. Hence the mass balance about 90 wt.%.

$$\text{Solid yield(carbon yield)} = \frac{\text{Mass of spent catalyst - mass of fresh catalyst}}{\text{Mass of plastic used}} \times 100\% \text{ (wt\%)} \quad (1)$$

$$\text{Oil yield (liquid yield)} = \frac{\text{Mass of spent condenser- mass of clean condenser}}{\text{Mass of plastic used}} \times 100\% \text{ (wt.\%)} \quad (2)$$

$$\text{H}_2 \text{ yield} = \frac{\text{Mass of H}_2 \text{ produced}}{\text{Mass of plastic used}} \left(\text{mmol g}_{\text{plastic}}^{-1}\right) \quad (3)$$

$$\text{Hydrogen efficiency} = \frac{\text{Total mass of H in hydrogen}}{\text{Theoretical mass of H in plastic}} \ (\%) \quad (4)$$

2.3Characterisation of pyrolysis products

Gaseous products were collected andquantified by gaschromatography (GC) (Panna

A91, China). To separate and analyse as many species as possible in the gas sample, two different modules, equipped with a thermal conductivity detector (TCD) and a flame ionisation detector (FID) were used.The TCD detector was used to detect the permanent gases, O_2, H_2, N_2, CO, and CO_2, using argon as the carrier gasata GC column temperature of 80°C.The FID detector was used to determine hydrocarbons, CH_4, C_2H_6, C_2H_4, and C_2H_2at a GC column temperature of 170 °C, and nitrogen was used as the carrier gas.The relative volume yields of the different gas compounds were calculated from the GC compositions. The LHV of the gaseous products was calculated usingEq.(5):

$$LHV(MJ/Nm^3)=0.126\times CO+0.108\times H_2+0.358\times CH_4+0.665\times C_nH_m \quad (5)$$

The crystalline structuresofthe fresh catalystswere determined by X-raydiffraction (XRD) (Philips X'Pert PRO, Japan)with a 2θ range of 15–80° and a scanning speed of $7°min^{-1}$.The crystal sizesof $Fe_2O_3$and Fe were calculated using theScherrer equation fromthe(1 1 0)and (1 0 4)lattice planes, respectively. The specific surface areas, total pore volumes,and pore size distributions of the catalysts were investigatedusingnitrogenadsorption measurements at 77 Kwith aBrunauer Emmett Teller (BET) analyser(Quantachrome IQ, America).

Gas chromatography-mass spectroscopy (Agilent 7890B/5977A, United States)was used to identify the components of the liquid product with an HP-5MD capillary column. To be exact, a 1-ml liquid sample was injected into the GCMS for detection. The GCMS parameters were set as follows: injection temperature of 300 °C, split ratio of 20:1, and carrier gas (He) flux in the column of 1 ml/min. The organic

components were further determined using mass spectral libraries (NIST14.L).

The particle size and surface morphology of all reacted catalysts were visualised through transmission electron microscopy (TEM)using a high-resolution transmission electron microscope (HR-TEM) (JEM-2100F, Japan).A thermogravimetric analysis (TGA) was conducted to analyse the thermal stability of the carbon productsdeposited on the catalyst during thecatalyticpyrolysis of polypropylene using temperature-programmed oxidation (TPO) from SetaramLabsys Evo1150 (China). For each test, approximately 10 mg of asolid carbonaceous material was heated to 800 °C under an air atmosphere (flow rate of 50 $mLmin^{-1}$) at a heating rate of 20 $°Cmin^{-1}$.Raman spectroscopywas applied to analyse the degree of graphitisationof the deposited carbon, scanning from 800 cm^{-1} to 3200 cm^{-1}, using a Raman instrument with an excitation wavelength of 532 nm(LabRAM HR 800 Evolution, France).In addition, the crystalline structures of the reacted catalystsweredeterminedthrough XRD.

3. Results and discussion

3.1 Characterisation of fresh catalysts

Theprepared solid fresh catalysts were characterised throughXRD and BET. The XRD patternsare shown in **Figure 2a**. The pure nano-Al_2O_3 support material exhibitedapproximately ten peaks at between $2\theta = 30°$ and 70°, among which four apparent peaks are located at $2\theta = 31.5°$, 32.8°, 59.9°, and 67.4° corresponding to the (0 0 4), (2 0 -2), (3 1 -3), and (2 1 5) planes of Al_2O_3.

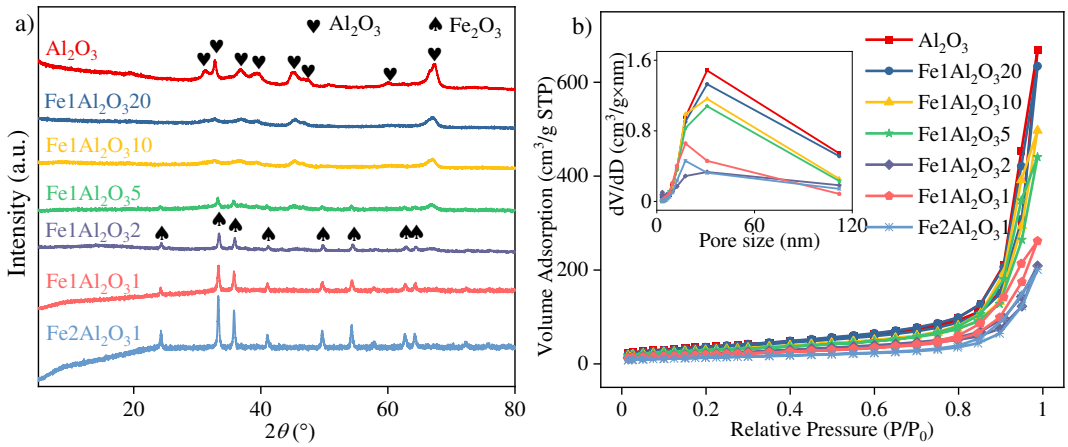

Figure 2.a) XRDdiffraction patternsand b) BET analysisof fresh Fe-based Al_2O_3 catalysts

However, with the introduction ofa small amount of Fe (Fe/Al_2O_3<1:5), the peaks for Al_2O_3apparently weakened, and several weakpeaks associated with Fe_2O_3were also observed.Upon further increasing the Fe content (Fe/Al_2O_3>1:5), several distinct cuspidal peakslocated at 2θ of 24.2°, 33.2 °, and 35.7°were observed, corresponding to the (0 1 2), (1 0 4), and (1 1 0) planes of Fe_2O_3, respectively(Aboul, 2018).This suggests that iron oxide crystallises more fully and exhibits a larger crystal size. As theFe content was further increased, there was no visible peak corresponding to Al_2O_3,and all peaks were related to Fe_2O_3. The exactcrystal size of the Fe-based species(Fe_2O_3), calculated from the peak position and half peak width,is shown in **Table 2**. As can be seen, thehalf-peak width decreased continuously with an increase in iron, corresponding to a better crystallinity. As expected, theaverage Fe_2O_3 particle size continued to increase, varying from approximately 13 to 65 nm, whichwas positively correlated with the added ironcontent.

Table 2

Crystal sizes of Fe_2O_3 and Fe of the fresh and reacted catalysts, respectively.

Sample	Fresh catalyst (Fe_2O_3)			Reacted catalyst (Fe)		
	peak position (^{o})	half peak width (^{o})	average size (nm)	peak position (^{o})	half peak width (^{o})	average size (nm)
Al_2O_3	-		-	-	-	-
Fe1$Al_2O_3$20	32.726	0.624	13.121	45.286	0.998	8.526
Fe1$Al_2O_3$10	32.780	0.603	13.576	45.670	0.857	9.951
Fe1$Al_2O_3$5	33.260	0.281	29.199	44.946	0.749	11.354
Fe1$Al_2O_3$2	33.412	0.250	32.861	44.627	0.374	22.681
Fe1$Al_2O_3$1	33.298	0.156	52.563	44.720	0.281	30.252
Fe2$Al_2O_3$1	33.292	0.125	65.702	44.732	0.25	34.035

The isothermal adsorptioncurves and pore size distributions of the fresh catalysts are shown in **Figure 2b**. As can be seen, all catalysts exhibitedtype II isotherms and H3 hysteresis loops, the latter at higher relativepressures (near 0.5–1.0), resulting in slit-type pores forming thestacking of plate-like particles, which is often seen in mesoporous materials,as presentedin previous studies(Cai, 2020a; Cai, 2020b; Cao, 2021).The specific surface areas (S_{BET}), pore volumes, and average porediametersof all Fe/Al_2O_3fresh catalysts are listed in **Table 3**. Apparently, when Fe was introduced, the surface area (S_{BET}) decreased gradually from pure Al_2O_3 at 130.6 $m^2 g^{-1}$ to 49.1 $m^2 g^{-1}$ for the Fe2$Al_2O_3$1 catalyst.

Table 3

Pore structure parameters of all fresh catalysts.

Sample	S_{BET} (m^2g^{-1})	V_{total} (cm^3g^{-1})	$D_{average}$ (nm)
Al_2O_3	130.65	1.04	31.74
Fe1$Al_2O_3$20	126.52	0.98	31.01
Fe1$Al_2O_3$10	106.37	0.77	28.99
Fe1$Al_2O_3$5	103.33	0.68	26.44
Fe1$Al_2O_3$2	78.08	0.43	26.04
Fe1$Al_2O_3$1	70.50	0.41	22.97
Fe2$Al_2O_3$1	49.06	0.31	25.32

The total pore volume and average pore diameter showed a similar tendency and decreased with an increase in the$Fe:Al_2O_3$ ratio. Both the highest total pore volume and average pore diameter were obtained for pure Al_2O_3, at 1.04 $cm^3\ g^{-1}$ and 31.74 nm, respectively. This suggests that the addition of Fe blocked some of the internal pores. This may be a disadvantage for catalytic reactions (Sun, 2018). In addition, the pore size distributions of the different fresh catalyst samples are shown in **Figure 2b** (inset). An obvious peak at approximately 30 nm, corresponding to a mesoporous structure, was observed, and the pore volume tended to decrease correspondingly. This was consistent with the total pore volume and average diameter data for the different catalysts, as presented in **Table 3**.

3.2Effect of Fe/Al_2O_3 on product distribution.

The product yield produced from the catalytic pyrolysis of the polypropylene waste is shown in **Figure 3**. The main products from the catalytic-pyrolysis of polypropylene withAl_2O_3alone weremainly gas (~45 wt.%) and liquid oil (~27

245 wt.%)with a limited solid carbondeposition(~16 wt.%). There was negligible char
246 residuefrom pyrolysis owing to the almost complete volatilisation of the
247 polypropylene used(Yao, 2017). With the introduction of Fe to Al_2O_3 ($Fe1Al_2O_320$),
248 the yield of solid carbondeposits increasedwith a corresponding decrease inthe liquid
249 oil yield. When the Fe content in the catalyst increased as the Fe
250 toAl_2O_3ratioincreased from 1:20 to 1:2, the yield of solid carbon deposits
251 increasedrapidly, whereas that of the liquid oil showed a corresponding decrease;
252 however, the gaseous product yield seemed to be relatively stable.It might suggest
253 that more hydrocarbons were converted into carbon deposits because of the increased
254 presence of Fe particles on the catalyst(Shen, 2014).In addition, the carbon deposits
255 yield obtained from $Fe1Al_2O_310$ was comparable to that obtained from other
256 research(Yao, 2018). A further increase in the Fe content of the catalysts showed that
257 the yield of different products exhibited a lower influence. The maximum yield of the
258 solid carbon deposit(approximately 42 wt.%) was obtained for the$Fe1Al_2O_31$ catalyst.
259 This means that a better catalytic activity of the Fe-based catalysts was obtained under
260 this condition, with a minimum liquid mass yield (3.3 wt.%). By contrast, further
261 increasing the ratio of Fe slightly reduced the yield of solidcarbon andincreased the
262 amount of liquid oil. This might be ascribed to the larger Fe particles in the catalyst,
263 which not only blocked the pores in the Al_2O_3support but also reducedthe catalytic
264 reactivity on the surface (Yang, 2019).The mass balance in all experiments was
265 calculated to be within the range of 88–96 wt.%.The mass loss can be attributed to the
266 pyrolysis vapors that condensed on the inner walls of the quartz reactor during the

catalytic pyrolysis process, also even some large hydrocarbon is difficult to vaporized and be detected with the GC system used in this study.

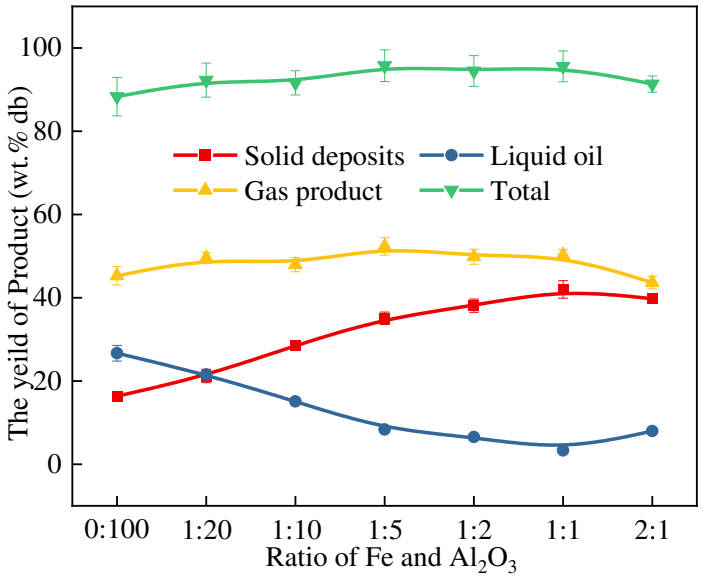

Figure 3. The yield of different products fromcatalytic-pyrolysis of polypropylene.

3.3 Composition of the gas products.

The composition of the gas derived from the catalytic pyrolysis of polypropylene with different catalysts is shown in **Figure 4**. As shown in **Figure 4a**, the gas products mainly contained small molecule hydrocarbons such as CH_4 (54.8 vol.%), C_2H_4 (20.5 vol.%) and a small quantity of C_2H_6 without the presence of Fe. Simultaneously, approximately 22.8 vol.% H_2 was also observed in a gaseous state. This is produced from the hydrogen abstraction reaction, a reaction mechanism that occurs during the pyrolysis of polypropylene and is necessary to break the chemical bonds of polypropylene and for the release of volatiles (CH_4, C_2H_4, andmacromolecular hydrocarbons) at high temperatures(Hu, 2020).Notably, propylene and some other larger gas molecules such as propane were produced during the catalytic

pyrolysisprocess. However, this is not reflected well in **Figure4a**owing to its limited content. The thermal decomposition process of polypropylene plastic can be described byEq. (6). It should be noted that no CO_2or CO was detected, which further illustrates the excellent chemical stability of the substrate Al_2O_3.

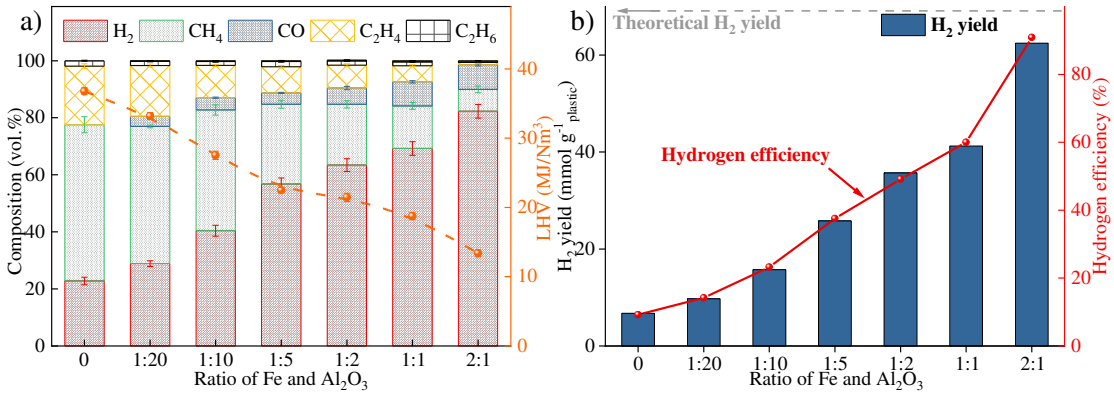

Figure 4. a) Gaseous product distribution and b) yield and efficiency of hydrogen obtained from thecatalytic-pyrolysis of polypropylene.

When theFe/Al_2O_3catalystswere introduced into the catalytic system, COwas detected, whichconfirmed that iron oxide was involved in the reaction and the oxygen from the $Fe_2O_3$was transferred tocarbon oxides. Asthe ratio of Fe increased, the volume fractions of CH_4 and C_2H_4 decreased and the H_2 content increased continuously. At the same time, CO increased with the increase in Fe content, which might be attributed to the factthat the catalytic reforming reaction was strengthened with Fe loading.The catalytic reforming process can be described as follows: First, Fe-based species (Fe_2O_3) were reduced to zero-valent iron usingH_2(Eq. (7)) or other reducing gases. Furthermore,the reduced iron metal particles could be in a quasi-liquid state and promote catalytic cracking reactions and decomposition of

hydrocarbons, resulting in a decrease in hydrocarbon gases and an increase in H_2 content(Aboul, 2018).Simultaneously,complex chemical reactions occur;hydrocarbons react with H_2O to release CO and H_2 (Eqs. (9) and (10)) (Yang, 2015),and awater–gas shift reactionmightoccur between C or CO and H_2O (Eq. (11))(Wu, 2009). All of these reactions result in an increase in H_2 content, which is associated with the final gaseous products. Ultimately, remnant C was converted into solid carbonin the presence of magnetic iron (Eq. (8))(Chen, 2001).In addition, the hydrogen content continually increased even when the ratio of Fe was higher than 50%. It has been reported that Fe can accelerate dehydrogenation reactions during catalytic process, leading to the increase of hydrogen simultaneously(Xia, 2019). Moreover, combining with the products distribution, inverse trend has been observed that more hydrogen was gathered but less carbon deposits were collected. This might indicate a quite different conversion process for waste PP with the presence of different ratio of iron catalysts.

$$(C_3H_6)_n \longrightarrow (CH_4+H_2+C_2H_4+C_2H_6+\times\times\times)+\text{oil} \quad (6)$$

$$Fe_2O_3+H_2 \longrightarrow Fe+H_2O \quad (7)$$

$$C_XH_y \xrightarrow{Fe} C+H_2 \quad (8)$$

$$C_XH_y+H_2O \longrightarrow CO+H_2 \quad (9)$$

$$CO+H_2O \longrightarrow CO_2+H_2 \quad (10)$$

$$C+H_2O \longrightarrow CO+H_2 \quad (11)$$

With respect to the LHV calculated from Eq. (5), the LHV of the gaseous productsproduced over theFe:Al_2O_3 catalysts decreased owing to the increase in

hydrogen content with the continuous increase in iron.However, all of the LHV values were still within the range of medium heating values and exceeded the minimum threshold value of 7 MJ Nm^{-3}as stipulated by the Chinese National Standard for fuel gas for urban residents (Gao, 2017), providing the possibility for a subsequent direct utilisation. As can be seen, theH_2 yield increased with the increase in Fe, and the maximum H_2 yield was ~62 mmol $g^{-1}_{plastic}$(**Figure 4b**), which was higher than that gathering from microwave-initiated catalytic deconstruction of 55.6 mmol $g^{-1}_{plastic}$(Jie, 2020). The theoretical H_2 yieldwas ~70 mmol $g^{-1}_{plastic}$ if the hydrogen in PP was fully transferred into H_2, which means that approximately90% hydrogen efficiency was obtained from the catalytic pyrolysis of PP, indicating that over 90% of the hydrogen contained in PP was extracted.This is pretty much higher than that obtained from other researches (Jie, 2020). There is no doubt that Fe based catalyst can promote the formation of CNTs, releasing hydrogen at the same time.Notably, the much higher hydrogen contained in the gaseous productscan alsobe further used for metallurgy, or as a hydrogen source for proton exchange membrane fuel cells after further processing(Khodakov, 2007).

3.4Properties of the liquid oil

The carbon chain length distributions of the organic constituents in the liquid oil product from thecatalyticpyrolysis of waste polypropylene in relation to the different Fe:Al_2O_3 catalysts used are illustrated in **Figure 5**. As can be seen, with pure Al_2O_3, the liquid oil obtained was rich in hydrocarbons (wax) or aromatics with a wide range

of carbon numbers, varying from C6 to C20.Notably, substances with larger carbon numbers could not be detected because of limitations to the instrumentation.The components in the liquid oil are relatively complex and consist of over half of the monocyclic and dicyclic aromatic compounds (Xu, 2020). In addition, a small number of compounds containingthree, four, or even five benzene rings, such as pyrene and benzo[e]pyrene, were also detected. Widespreadaromatic compounds can be formed throughthe Diels–Alder reaction and dehydrogenation process (Park, 2019a). In addition, the presence of Lewis acid sites within the catalysts also contributed to the formation of aromatic compounds, especially for the liquid oil obtained from Fe/ZSM-5. Furthermore, acid sites are significantly conducive to the formation of carbon deposits, which are the major source of amorphous carbon (Che, 2019).

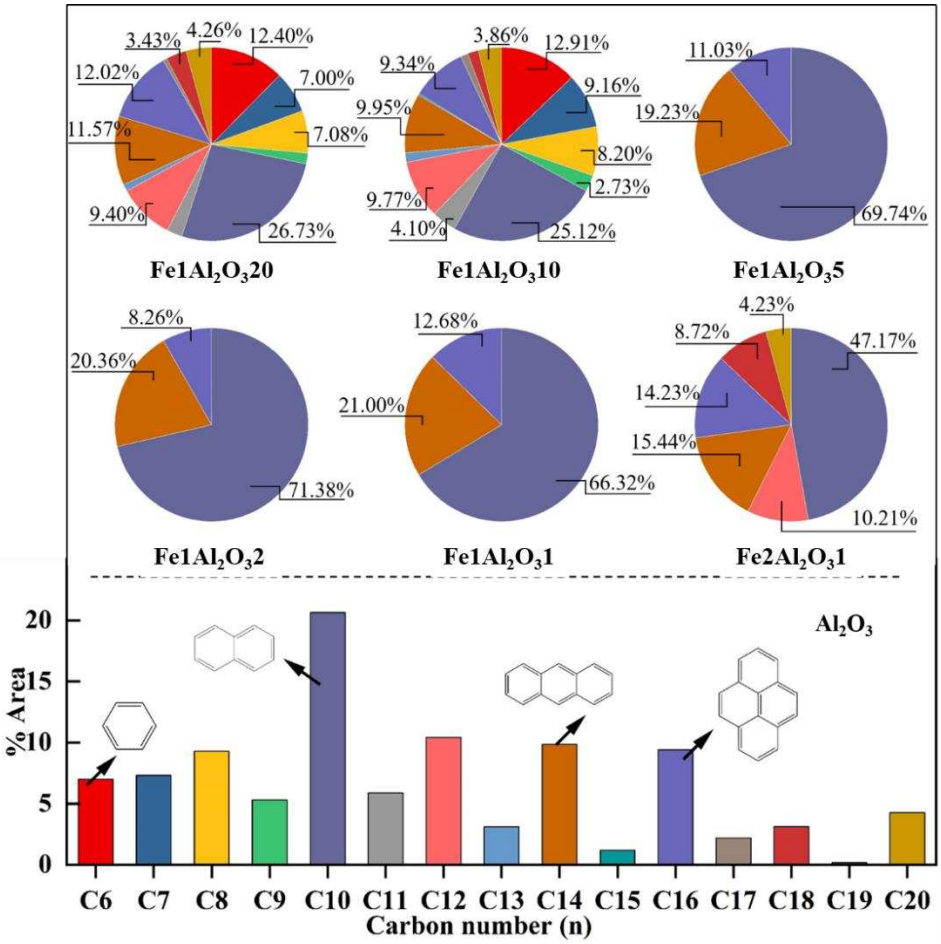

353

354 **Figure 5**. Carbon distribution of liquid oil fromcatalytic-pyrolysis of polypropylene

355 with different catalysts.

356 In the case of catalysts containing Fe,the carbon number range of the compounds

357 contained in the liquid oil was almost unchanged, and only small changes were

358 observed in the liquid composition when thecontent of Fe was less than 10% (the ratio

359 of Fe to $Al_2O_3$was less than 1:10.For example, there was an increase in benzene and

360 naphthalene and a decrease in xylene and 2-methyl naphthalene. It may be suggested

361 that, in the presence ofacatalyst,thebranched chainonxylene or 2-methyl

362 naphthalenewas removed, and more stable substances such as benzene and

363 naphthalene were formed.Whenthe ratio of Fe to Al_2O_3reached1:5, the composition of

the liquid oil collected changed significantly, and only three types of organic compounds were detected,and the corresponding carbon numbers wereC10, C14, and C16, corresponding to naphthalene, anthracene, and pyrene, respectively. It is worth noting that naphthalene, anthracene, and pyrene were present with no branch chains, which suggests that the existence of iron catalyst can not only promote Diels–Alder reaction fromchain hydrocarbon but facilitate the removing of branches, leading to the formation of more stable aromatic compounds like naphthalene without branches. Moreover, these aromatic compounds are thought to be precursors for the formation of carbon layers(Park, 2019b). Moreover, **Figure 5**shows that naphthalene comprised more than 70% of the composition of the product oil fromtheFe1$Al_2O_3$2 catalyst. Naphthalene is one of the most important polycyclic aromatic hydrocarbons used in industry,and such a high concentration produced during the process can be attractive owing to its commercial recovery(Bendebane, 2010). However, with a further increase in the Fe to Al_2O_3ratio, the number of aromatic compounds with more than 16 carbon numbersfurther increased, leading to the simultaneous release of hydrogen, which was consistent withthegaseous results.This suggests that too much metal introduced in the catalysts reduced the reactivity, resulting in a deterioration in the quality of the liquid product. There are plenty of PAHs in liquid oil, whichplay a major role in the bio-oil quality (Wang, 2020). It is possible for liquid oilto be applied as additives to jet fuel after further chemical refinement(Lakshmikandan, 2021).

3.5Structure of solid carbon deposits

The carbon deposits on the catalyst produced from the catalytic pyrolysis of polypropylene in relation to the different Fe:Al_2O_3 catalysts were further characterised and analysed. A TEM analysis was conducted, and TEM images of the carbon deposits are as shown in **Figure6**.

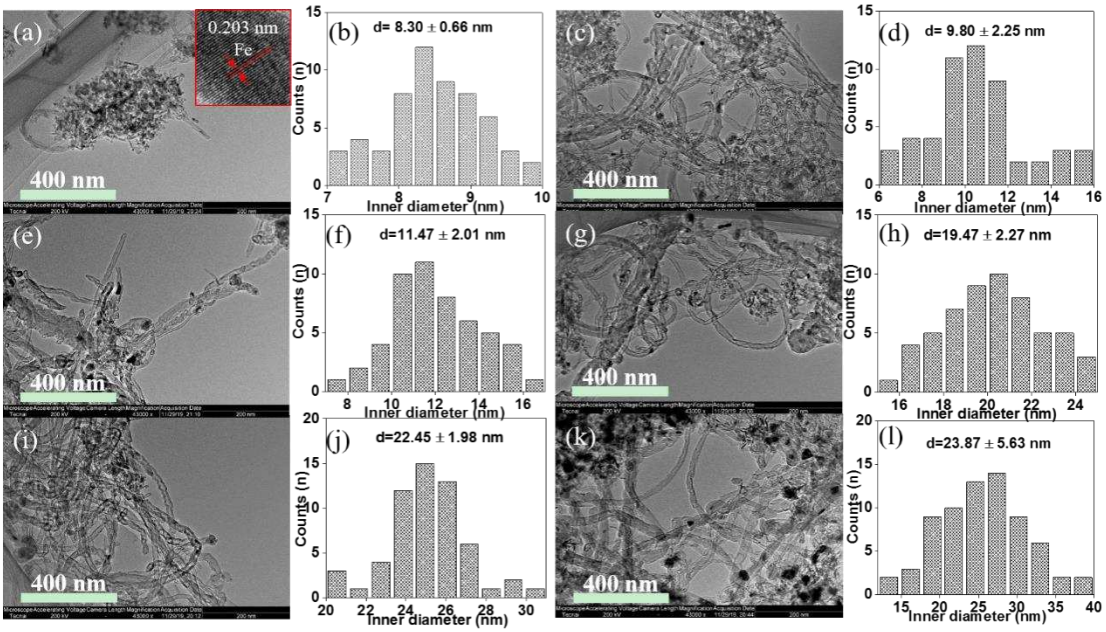

Figure 6.TEM imagesand inner diameter distributionof solid carbondeposits fromthecatalytic-pyrolysis of polypropylene in relation to the different Fe:Al_2O_3catalysts. (a, b) Fe1$Al_2O_3$20,(c, d)Fe1$Al_2O_3$10, (e, f)Fe1$Al_2O_3$5, (g, h)Fe1$Al_2O_3$2, (i, j)Fe1$Al_2O_3$1,and (k, l)Fe2$Al_2O_3$1.

The deposited carbon materials were mainly of afibrous type, the length of which varied from approximately 100 nm to several microns. To be exact, for carbon deposition on aFe1$Al_2O_3$20 catalyst (**Figure 6a**),many claviformsubstances related to the support materialcan be observed.In addition, a small number of carbon nanotubes

398 with metal nanoparticles insidecan be clearlyobserved,with a lattice size of 0.203nm,
399 which corresponds to Fe, furtherproving that it participated in the process of reduction
400 and the formation of the CNTs(He, 2021). By increasing the ratio of Fe, a large
401 number ofCNTsintertwiningwith each other canclearly be seen (**Figure6c**).With a
402 further increase inthe ratio of Fe to Al_2O_3, the observable carbon was almost entirely
403 made up of CNT materials, and littleclaviformAl_2O_3 was observed(**Figure 6e**, **g**,**i**,and
404 **k**). Notably, a fewirregular black substances can be observed for the reacted
405 Fe2$Al_2O_3$1 catalyst,which were attributed to the large iron particles produced fromthe
406 reduction process(**Figure 6k**), originating from the excess introduction of iron.As
407 shown in **Figure 6**, it seems that catalysts with lower Fe ratiosled totip-growthowing
408 to the widespread presence of metal particles in the middle of the CNTs. By contrast,
409 almost no metal particles could be seen in the middle or top of the CNTs obtained
410 foranFe catalyst with a higher ratio (>1:1), which means thatthe base-growth
411 mechanism dominated the growth process of the CNTs. This might be related to the
412 different interactions between the active metal and the substrate material. Furthermore,
413 the stress limitation of the carbon formation process may also lead to the diversity of
414 formation mechanisms.
415 The inner diameter distribution and standard deviation analysis of the CNTs
416 produced were calculated usinga mathematical and statistical analysis(**Figure 6**).
417 Clearly, the carbon deposits on the Fe1$Al_2O_3$20 catalyst (**Figure 6b**) were thinner than
418 those on the other catalysts, and the average inner diameter was approximately 8.30
419 nm. In addition, the smalleststandard deviation was obtained with the

Fe1$Al_2O_3$20catalyst, reflecting the uniform distribution of the CNTs. As shown in**Figure 6b**, **d**, **f**, **h**, **j**,and **l**, the average inner diameter (between 9.80 and 23.87 nm) increased with the increase in Fe content, and the results were consistent with the size of the iron particles (**Figure 7a** and**b**). However, there weresome gaps in the values between the average inner diameter and the particle size,which might be due tothevariety of carbon layers and the Fe particle size from atensile deformation and self-stress of the original unstable larger particles(Lin, 2007). Therefore, the inner diameters of the carbon nanotubes were smaller than the average size of the iron particles with respect to the large size of the reduced Fe particles. Similar results have been obtained by other researchers (Liu, 2018).For example, Cheung et al. (Cheung, 2002)obtained CNTs with average diameters of 3, 7, and 12 nm from ethylene usingFenanoparticlecatalysts with average diameters of 3, 9, and 13 nm,respectively. In addition, almost no amorphous or disordered carbon was observed in the reacted Fe-based catalysts, which further confirmed the importance of iron in the growth of CNTs.

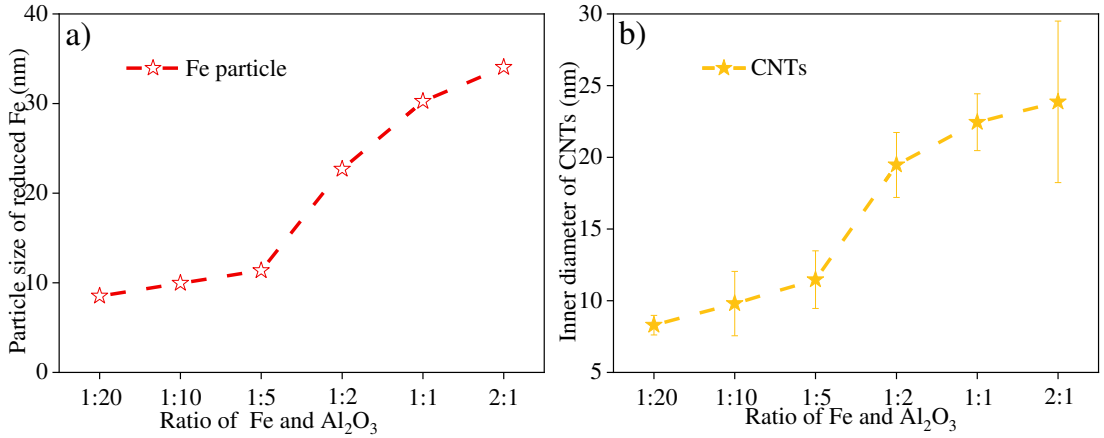

Figure 7.a) Diameter comparison for reduced Fe particles and b) the produced carbon

nanotubes.

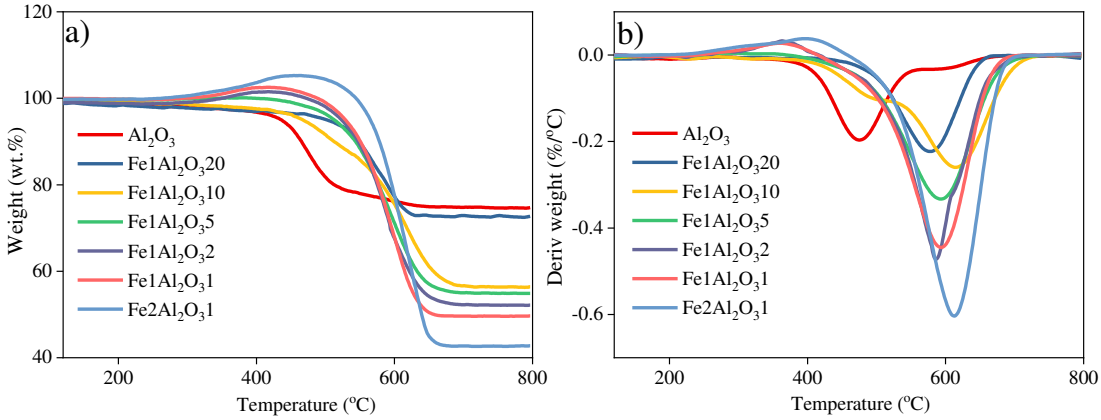

Figure 8.a) Thermogravimetric analysis (TGA) and b) derivative thermogravimetry (DTG) of the solid deposits obtained from thecatalytic-pyrolysis of polypropylene.

Temperature-programmed oxidisation (thermogravimetric analysis (TGA) and derivative thermogravimetry (DTG)) was applied for the different reacted Fe: Al_2O_3 catalysts, the results of which are shown in**Figure 8**.As shown in **Figure 8a**,the carbon deposits on the reacted pure Al_2O_3 revealed a significant thermal stability at temperaturesof lower than 400°C, which can be ascribed to the stability and high crystallinity of the carbon materials(Zhang, 2015). When the temperature was increased to 400 °C, the carbon began to oxidise and underwenta rapid weight loss stage between 400 °C and 500°C,representinga weight loss ofapproximately 25% of the initial weight. Anobvious weight loss peak could be observed from the DTG curve associated with reacted Al_2O_3at approximately 475 °C (**Figure 8b**), whichcould be related to the oxidation of amorphous carbon, which was not as stable as graphite carbon(Yang, 2015). As the reaction temperature was further increased to approximately 600 °C, a slower rate of weight loss was observed, which might be

related to the oxidation of a small amount of graphite-typecarbon, which has a higher thermal stability.There was an inflection point, located in around 550 °C, between the two-combustion process and this can be used as the diacritical point ofamorphous and graphite carbon. Apparently, pretty much more amorphous carbon was gathered from pure Al_2O_3 catalyst.When Fe was introduced into the catalysts, the temperature at the start of weight loss and weight loss peak temperature shifted to higher temperatures (over 100 °C).With an increase inthe ratio of Fe to Al_2O_3, the maximum weight loss continued to increase. Apparently, the weight loss peaks of the reacted Fe/Al_2O_3catalysts were at higher temperatures of approximately 600°C, and the peak strength increased with an increase in theiron ratio.This was ascribed to the widely formed graphite carbon (mainly CNTs, as shown in **Figure 6**). Notably, the TG method can only be used to estimate the amount of different types of carbon, while the structure in detail should refer to other advance instruments.In addition, when the ratios of Fe and Al_2O_3 were 1:2, 1:1, and 2:1, there was a slight mass increase at approximately 400 °C to 500°C, which was associated with a fairly high content of iron and the corresponding oxidation during the high-temperature TGA process(Wu, 2009).At the end of the TPO analysis, the residual mass of the solid powder remaining in the crucible was consistent with the yield shown in **Figure 3**, and the main components werealuminium oxide or a mixture of iron and aluminium oxides(Cai, 2021).

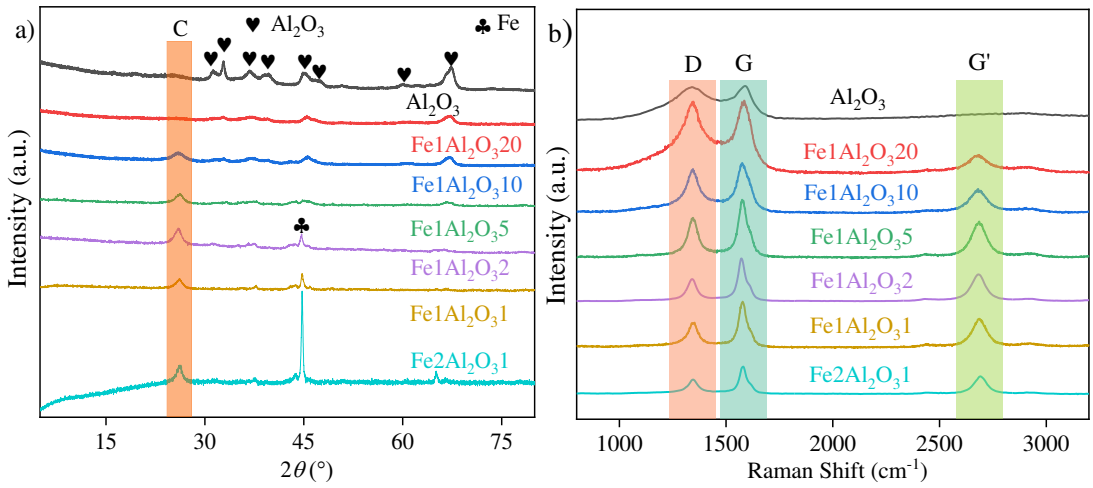

Figure 9. a) XRD diffraction patterns and b) Raman spectroscopy of the solid deposit residue from thecatalytic-pyrolysis of polypropylene.

The physical structure of the reacted catalysts was further examinedthrough XRD (**Figure 9a**), and the crystal sizes of the iron particles insidewere calculated (**Table 2**).The diffraction peaks of the reacted Al_2O_3 appeared to be similar to that offresh Al_2O_3, which further reflected thethermal stability of Al_2O_3. Almost all peaks were associated with Al_2O_3, and no obvious peak associated with carbon was presentbecause of the small amount of amorphous carbon deposited. Withthe addition ofa small amount of Fe ($Fe1Al_2O_320$), the peaks for Al_2O_3 became much weaker. Simultaneously, the carbon peak was difficult to detect owing to its relativelylow degree of graphitisation. When the ratio of Fe to Al_2O_3 was increasedto 1:10, an obvious broad carbon peak was observed at 2θ =26.3°, indicatingthatthemetal species played an indispensable role in theformation of graphite carbon. Furthermore, the presence of iron, originating from the reduction of ferric oxide, was confirmedby themain peak at 2θ of the 44.7°peak when the Fe content was sufficientlyhigh ($Fe1Al_2O_32$,$Fe1Al_2O_31$,and$Fe2Al_2O_31$). Our previous study also confirmed that

hematite was initially reduced to magnetite at lower temperatures (approximately 400 °C), and further, the magnetite was reduced into unstable wustite and finallyiron with the consumption of the reducing gas(H_2) (Yao, 2018).The crystal size of the reducedFe particles increased with the increase in the Fe content,varying from 8.526 to 34.035 nm (**Table 2**). Combining the results discussed above, the particle size plays a key role in the catalytic reforming waste plastics process, which not only determines the yield of various products, but also affects their composition and properties.

The degree ofgraphitisation ofthe carbon deposit on the reacted catalysts was evaluated usinga Raman spectrometry analysis, the results of which are shown in **Figure 9b** and **Table 4**. Three peaks wereobserved at approximately 1340 cm^{-1} (D band), 1580 cm^{-1} (G band), and 2670 cm^{-1} (G' band)in the Raman spectra. The Dband corresponds to the amorphous or sp^3 disordered structure in the carbon materials, which is associated with finite graphitic planes and some other forms of carbon such as carbon rings with defects(Sveningsson, 2014). The G band is usually attributed to the planar motion of ordered sp^2-hybridised carbon atoms in the graphite layers, which isclosely related to the degree of graphitisationof the carbon materials, and the G' band is connected with the stacking order of carbon atoms(Chernyak, 2019). The number of disordered and defective sites in the carbon structure can be estimated from the relative peak intensity ratio of the D to G bands (I_D/I_G), and the larger I_D/I_G ratio, which is related to a lower degree of graphitisation. As shown in **Table 4**, the I_D/I_G value of thecarbon deposits on the reacted Al_2O_3 was 0.98, indicating a relatively low graphitisation. With an increase in the Fe content in the catalysts, the value of

513 I_D/I_Gexhibited a tendency todecrease, which implied that the existence of Fepromoted
514 the formation of graphite layers and increased the degree of graphitisation. In addition,
515 the intensity ratio $I_{G'}/I_G$isfrequentlyused to describe the existence and purity of the
516 carbon nanotubes produced, and a higher intensity of the $I_{G'}/I_G$ratio corresponds to a
517 higher purity(Yao, 2018). As for the reacted Al_2O_3, only D and G bandscould be
518 detected, which could be ascribed to the widespread presence of amorphous carbon.
519 For the carbon deposits obtained from the Fe-based catalysts, an apparent G' peak was
520 observed at approximately 2750 cm^{-1}, which further reflected the formation of CNTs.
521 The values of $I_{G'}/I_G$ for the reacted $Fe1Al_2O_320$, $Fe1Al_2O_310$, $Fe1Al_2O_35$, $Fe1Al_2O_32$,
522 $Fe1Al_2O_31$, and $Fe2Al_2O_31$ catalysts were 0.32, 0.52, 0.64, 0.65, 0.66, and 0.68,
523 respectively, which might mean that there is an increase in the purity of the CNTs with
524 increasing Fe content. This is supported by the TG results, which showed that the
525 solid deposit from the catalysts with a higher Fe content lost more weight at TPO
526 temperatures ofabove 600 °C.

527 However, according to the results reported above, it seems that the continuous
528 introduction of Fe does not result in significantlyenhanced catalytic effects. The
529 introduction of high iron content not only decreases the specific surface area of the
530 catalystsbut also forms larger metal particles. Both of these factors leadto a decrease
531 in the catalyst activity, which results in an unsatisfactory performance(Zhou,
532 2014).Therefore, it is important to select a suitable metal load to achieve a good
533 catalytic effect.

534 **Table 4**

Degree of graphitisation of solid deposits from thecatalytic-pyrolysis of polypropylene.

Reacted Catalyst	Al_2O_3	Fe1 $Al_2O_3$20	Fe1 $Al_2O_3$10	Fe1 $Al_2O_3$5	Fe1 $Al_2O_3$2	Fe1 $Al_2O_3$1	Fe2 $Al_2O_3$1
I_D/I_G	0.98	0.99	0.89	0.69	0.54	0.58	0.57
$I_{G'}/I_G$	-	0.32	0.52	0.65	0.64	0.66	0.68

In order to further this catalytic pyrolysis process, more analysis was introduced. Based on experiments and corresponding data,preliminary material flow was presented (Figure 10). Starting from 1 g plastic sample, up to 42 wt.% of the feedstock can be converted to carbon deposits with the presence of iron catalyst (Fe1$Al_2O_3$1), which is comparable to that obtained from bimetallic catalyst(Yao, 2017). Thereinto, pretty much higher purity of CNTs, over 300 mg, can be gathered. Simultaneously, approximately 50 wt.% gaseous products and over 82 mg hydrogen were collected. In addition, liquid products were rich in aromatic hydrocarbons, in which the selectivity of naphthalene is more than 60 area% from Fe1$Al_2O_3$1 catalyst.

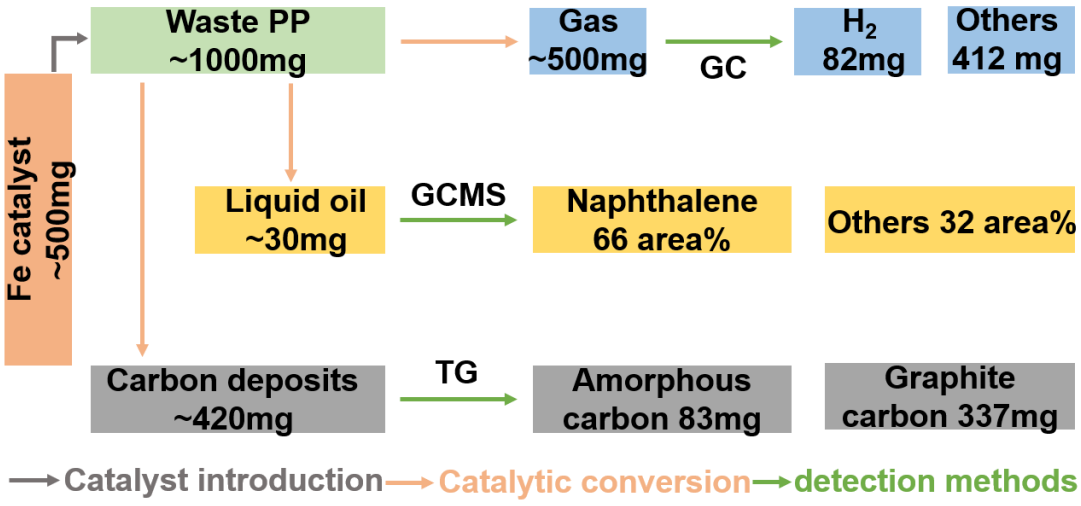

Figure 10. Material flow of the catalytic pyrolysis process

548 In order to further identify the economic viability, the cost breakdown of the
549 process has been presented in Table 5. The costs of catalytic pyrolysis were mainly
550 calculated by the price of plastic sample, catalyst, electricity water and workers(Li,
551 2018). The raw data was obtained from experimental data in this work, biomass
552 pyrolysis (Xia et al., 2018) and polygeneration system(Gao, 2017). Notably, the initial
553 capital investment and equipment depreciation were neglected because the process is
554 the main consideration. Apparently, catalyst and electricity accounted for the most
555 two parts in the process, and both of these accounted for more than 90 percent of cost.
556 To be exact, they were 50k USD and 47k USD, respectively. As mentioned before, the
557 catalytic properties of iron catalyst are comparable to that of bimetallic catalyst like
558 nickle-iron. Moreover, the additional use of other transition metal like nickel or cobalt
559 inevitably increase the cost of the thermal conversion technology. As a result,
560 inexpensive iron-based catalyst adds a promising option with excellent efficiency for
561 hydrogen, aromatics and CNTs productions from waste resources.

562 Table 5 The raw cost data of catalytic pyrolysis waste PP.

Number	Item	
1	Plastic sample for catalytic pyrolysis (t/y)	100
2	Price of plastic sample (USD/t)	60
3	Catalyst for catalytic pyrolysis (t/y)	50
4	Price of catalyst used (USD/t)	1100
5	Electricity (kwh/year)	426573
6	Price of electricity (USD/t)	0.11
7	Water (t/year)	120
8	Price of water (USD/t)	0.0756

9	Number of people	2
10	Salary (USD/y)	5000
11	Total (USD/y)	117932

4 Conclusions

In this paper, the characteristics of the products and possible reaction mechanisms were discussed for catalytic-pyrolysis waste PP in the presence of iron catalysts at 800 °C. The introduction of iron metal to catalysts can dramatically suppress the formation of liquid oil, promote the generation of carbon deposits, and release large amounts of hydrogen simultaneously. When the ratio of Fe/Al_2O_3 catalyst was 1:1, the maximum yield (~42 wt.%) was obtained. Simultaneously, around 50 wt.% gaseous products and less than 5 wt.% liquid oil were gathered. The carbon deposits contained abundant CNTs with high degree of graphitisation, and the inner diameters varied from a few to dozens of nanometres. The growth mechanism of CNTs follows a top-growth and base-growth mechanism and this is related to the size of the metal particles. Gaseous products contained more hydrogen than other components. To be exact, over 60 vol.% hydrogen and almost 60% hydrogen efficiency was obtained from the catalyst with ratio of 1:1). In addition, high selectivity of naphthalene (over 60 area%) and aromatics was detected for liquid oil, it is possible for further application after purification.

For prospective insight, more efforts should be made to determine the reaction mechanism and clarify the strategy of product quality control. In addition, the current research was mainly at the laboratory scale, andpilot-scale experimental research

should be carried out for accelerating industrialization.Moreover, both real plastic waste andlifecycle assessmentsshould also be introducedto the process of ongoing research to determine the feasibility of practical application so that the commercialised utilisation of waste plastics can be come true.

Acknowledgements

The authors wish to express their sincere thanks for the financial support from the National Key Research and Development Program of China (2018YFC1901204), the National Natural Science Foundation of China (51806077 and 51861130362), China Postdoctoral Science Foundation (2018M640696) and the Foundation of the State Key Laboratory of Coal Combustion (FSKLCCB2001). The testswere also assisted by the Analytical and Testing Center in Huazhong University of Science & Technology (http://atc.hust.edu.cn, Wuhan 430074 China) and ZHONG KE BAI CE (http://www.zkbaice.com/).

References

Abdul-Wahab, M., JacksonS D. 2013. Hydrogenation of 3-nitroacetophenone over rhodium/silica catalysts: Effect of metal dispersion and catalyst support. *Appl. Catal., A*, **462-463**, 121-128.http://dx.doi.org/10.1016/j.apcata.2013.05.002.

Aboul, A., Awadallah A. 2018. Production of nanostructured carbon materials using Fe–Mo/MgO catalysts via mild catalytic pyrolysis of polyethylene waste. *Chem. Eng. J.*, **354**, 802-816.https://doi.org/10.1016/j.cej.2018.08.046.

Barbarias, I., Lopez G, Artetxe M, Arregi A, Bilbao J, Olazar M. 2018. Valorisation of different waste plastics by pyrolysis and in-line catalytic steam reforming for hydrogen production. *Energy Convers. Manage.*, **156**, 575-584.https://doi.org/10.1016/j.enconman.2017.11.048.

Bendebane, F., Bouziane, L, Ismail, F. 2010. Extraction of naphthalene. Optimization and application to an industrial rejected fuel oil. *J. Ind. Eng. Chem.*, **16**(2), 314-320.https://doi.org/10.1016/j.jiec.2010.01.033.

Bora, R., Wang R, You F. 2020. Waste Polypropylene Plastic Recycling toward Climate Change Mitigation and Circular Economy: Energy, Environmental, and Technoeconomic Perspectives. *ACS Sustainable Chemistry & Engineering*, **8**(43), 16350-16363.https://dx.doi.org/10.1021/acssuschemeng.0c06311.

Cai, N., Li Xi, Xia S, Sun L, Hu J, Bartocci P, Fantozzi F, Williams P, Yang H, Chen H. 2021. Pyrolysis-catalysis of different waste plastics over Fe/Al2O3 catalyst: High-value hydrogen, liquid fuels, carbon nanotubes and possible reaction mechanisms. *Energy Convers. Manage.*, **229**, 113794.https://doi.org/10.1016/j.enconman.2020.113794.

Cai, N., Xia S, Zhang X, Meng Z, Bartocci P, Fantozzi F, Chen Y, Chen H, Williams P, Yang H. 2020a. Preparation of Iron- and Nitrogen-Codoped Carbon Nanotubes from Waste Plastics Pyrolysis for the Oxygen Reduction Reaction. *ChemSusChem*, **13**(5), 938-944.http://dx.doi.org/10.1002/cssc.201903293.

Cai, N., Yang H, Zhang X, Xia S, Yao D, Bartocci P, Fantozzi F, Chen Y, Chen H, Williams P. 2020b. Bimetallic carbon nanotube encapsulated Fe-Ni catalysts from fast pyrolysis of waste plastics and their oxygen reduction properties. *Waste Manag.*, **109**, 119-126.https://doi.org/10.1016/j.wasman.2020.05.003.

Cao, B., Yuan J, Jiang D, Wang S, Barati B, Hu Y, Yuan C, Gong X, Wang Q. 2021. Seaweed-derived biochar with multiple active sites as a heterogeneous catalyst for converting macroalgae into acid-free biooil containing abundant ester and sugar substances. *Fuel*, **285**, 119164.https://doi.org/10.1016/j.fuel.2020.119164.

Che, Q., Yang M, Wang X, Yang Q, Williams L, Yang H, Zou J, Zeng K, Zhu Y, Chen Y, Chen H. 2019. Influence of physicochemical properties of metal modified ZSM-5 catalyst on benzene, toluene and xylene production from biomass catalytic pyrolysis. *Bioresour Technol*, **278**, 248-254.https://doi.org/10.1016/j.biortech.2019.01.081.

Chen, D., Christensen K, Ochoafernandez E, Yu Z, Totdal B, Latorre N, Monzon A,

Holmen A. 2005. Synthesis of carbon nanofibers: effects of Ni crystal size during methane decomposition. *J. Catal.*, **229**(1), 82-96.https://doi.org/10.1016/j.jcat.2004.10.017.

Chen, J., Li Y, Ma Y, Qin Y, Liu C. 2001. Formation of bamboo-shaped carbon filaments and dependence of their morphology on catalyst composition and reaction conditions. *Carbon*, **39**, 1467–1475.https://doi.org/10.1016/S0008-6223(00)00274-8.

Chen, W., Chen Y, Yan H, Li K, Chen X, Chen H. 2018. Investigation on biomass nitrogen-enriched pyrolysis: Influence of temperature. *Bioresour Technol*, **249**, 247-253.http://www.ncbi.nlm.nih.gov/pubmed/29049983.

Chernyak, S., Ivanov A, Stolbov D, Egorova T, Maslakov K, Shen Z, Lunin V, Savilov S. 2019. N-doping and oxidation of carbon nanotubes and jellyfish-like graphene nanoflakes through the prism of Raman spectroscopy. *Appl. Surf. Sci.*, **488**, 51-60.https://doi.org/10.1016/j.apsusc.2019.05.243.

Cheung, C., Kurtz A, Park H, Lieber C. 2002. Diameter-Controlled Synthesis of Carbon Nanotubes. *J. Phys. Chem. B*, **106**, 2429-2433.https://doi.org/10.1021/jp0142278.

Faisal, A., Daud W, Ashri W. 2014. A review on co-pyrolysis of biomass: An optional technique to obtain a high-grade pyrolysis oil. *Energy Convers. Manage.*, **87**, 71-85.http://dx.doi.org/10.1016/j.enconman.2014.07.007.

Gao, Y., Wang X, Chen Y, Li P, Liu H, Chen H. 2017. Pyrolysis of rapeseed stalk: Influence of temperature on product characteristics and economic costs. *Energy*, **122**, 482-491.http://dx.doi.org/10.1016/j.energy.2017.01.103.

Geyer, R., Jambeck J, Law K. 2017. Production, use, and fate of all plastics ever made. *Sci. Adv.*, **3**, 1-5.https://doi.org/10.1126/sciadv.1700782.

He, S., Xu Y, Zhang Y, Bell S, Wu C. 2021. Waste plastics recycling for producing high-value carbon nanotubes: Investigation of the influence of Manganese content in Fe-based catalysts. *J. Hazard. Mater.*, **402**, 123726.https://doi.org/10.1016/j.jhazmat.2020.123726.

Hu, Q., Tang Z, Yao D, Yang H, Shao J, Chen H. 2020. Thermal behavior, kinetics and gas evolution characteristics for the co-pyrolysis of real-world plastic and tyre wastes. *J. Cleaner Prod.*, **260**, 121102.https://doi.org/10.1016/j.jclepro.2020.121102.

Janardhan, H., Shanbhag G, Halgeri A. 2014. Shape-selective catalysis by phosphate modified ZSM-5: Generation of new acid sites with pore narrowing. *Appl. Catal., A*, **471**, 12-18.http://dx.doi.org/10.1016/j.apcata.2013.11.029.

Jia, J., Veksha A, Lim T, Lisak G. 2020. In situ grown metallic nickel from X–Ni (X=La, Mg, Sr) oxides for converting plastics into carbon nanotubes: Influence of metal–support interaction. *J. Cleaner Prod.*, **258**, 120633.https://doi.org/10.1016/j.jclepro.2020.120633.

Jie, X., Li W, Slocombe D, Gao Y, Banerjee I, Gonzalez-Cortes S, Yao B, AlMegren H, Alshihri S, Dilworth J, Thomas J, Xiao T, Edwards P. 2020. Microwave-initiated catalytic deconstruction of plastic waste into hydrogen and high-value carbons. *Nature Catalysis*, **3**(11),

902-912.https://doi.org/10.1038/s41929-020-00518-5.
Jin, L., Si H, Zhang J, Lin P, Hu Z, Qiu B, Hu H. 2013. Preparation of activated carbon supported Fe–Al2O3 catalyst and its application for hydrogen production by catalytic methane decomposition. *Int. J. Hydrogen Energy*, **38**(25), 10373-10380.http://dx.doi.org/10.1016/j.ijhydene.2013.06.023.
Khodakov, A., Chu W, Fongarland P. 2007. Advances in the Development of Novel Cobalt Fischer−Tropsch Catalysts for Synthesis of Long-Chain Hydrocarbons and Clean Fuels. *Chem. Rev.*, **107**, 1692−1744.https://doi.org/10.1021/cr050972v.
Kumagai, S., Hosaka T, Kameda T, Yoshioka T. 2017. Removal of toxic HCN and recovery of H2-rich syngas via catalytic reforming of product gas from gasification of polyimide over Ni/Mg/Al catalysts. *J. Anal. Appl. Pyrolysis*, **123**, 330-339.http://dx.doi.org/10.1016/j.jaap.2016.11.012.
López, A., Marco I, Caballero B, Laresgoiti M, Adrados A, Aranzabal A. 2011. Catalytic pyrolysis of plastic wastes with two different types of catalysts: ZSM-5 zeolite and Red Mud. *Appl. Catal. B: Environ.*, **104**(3-4), 211-219.http://dx.doi.org/10.1016/j.apcatb.2011.03.030.
Lakshmikandan, M.W., S. Murugesan, A. G. Saravanakumar, M. Selvakumar, G. 2021. Co-cultivation of Streptomyces and microalgal cells as an efficient system for biodiesel production and bioflocculation formation. *Bioresour Technol*, **332**, 125118.http://www.ncbi.nlm.nih.gov/pubmed/33866154.
Li, K., Lei J, Yuan G, Weerachanchai P, Wang J, Zhao J, Yang Y. 2017. Fe-, Ti-, Zr- and Al-pillared clays for efficient catalytic pyrolysis of mixed plastics. *Chem. Eng. J.*, **317**, 800-809.http://dx.doi.org/10.1016/j.cej.2017.02.113.
Li, S.C., G. 2018. Thermogravimetric, thermochemical, and infrared spectral characterization of feedstocks and biochar derived at different pyrolysis temperatures. *Waste Manag*, **78**, 198-207.https://doi.org/10.1016/j.wasman.2018.05.048.
Lin, M., Tan J, Boothroyd C, Loh K, Tok E, Foo Y. 2007. Dynamical Observation of Bamboo-like Carbon Nanotube Growth. *Nano Lett.*, **7**, 2234-2238.https://doi.org/10.1021/nl070681x.
Liu, X., Shen B, Wu Z, Parlett C, Han Z, George A, Yuan P, Patel D, Wu C. 2018. Producing carbon nanotubes from thermochemical conversion of waste plastics using Ni/ceramic based catalyst. *Chem. Eng. Sci.*, **192**, 882-891.https://doi.org/10.1016/j.ces.2018.07.047.
Miandad, R., Barakat, M. A., Rehan, M., Aburiazaiza, A. S., Ismail, I. M. I., Nizami, A. S. 2017. Plastic waste to liquid oil through catalytic pyrolysis using natural and synthetic zeolite catalysts. *Waste Manag*, **69**, 66-78.http://dx.doi.org/10.1016/j.wasman.2017.08.032.
Park, K., Jeong Y, Guzelciftci B, Kim J. 2019a. Characteristics of a new type continuous two-stage pyrolysis of waste polyethylene. *Energy*, **166**, 343-351.https://doi.org/10.1016/j.energy.2018.10.078.
Park, Y., Lee B, Lee H, Watanabe A, Jae J, Tsang Y, Kim Y. 2019b. Co-feeding effect of waste plastic films on the catalytic pyrolysis of Quercus variabilis over

microporous HZSM-5 and HY catalysts. *Chem. Eng. J.*, **378**, 122151.https://doi.org/10.1016/j.cej.2019.122151.

Prata, J.C.S., A. L. P. Walker, T. R. Duarte, A. C. Rocha-Santos, T. 2020. COVID-19 Pandemic Repercussions on the Use and Management of Plastics. *Environ Sci Technol*, **54**(13), 7760-7765.https://dx.doi.org/10.1021/acs.est.0c02178.

Ramadhani, B., Kivevele, T, Kihedu, J, Jande, Y. 2020. Catalytic tar conversion and the prospective use of iron-based catalyst in the future development of biomass gasification: a review. *Biomass Conversion and Biorefinery*.https://doi.org/10.1007/s13399-020-00814-x.

Rodriguez, E., Gutierrez A, Palos R, Vela F, Arandes J, Bilbao J. 2019. Fuel production by cracking of polyolefins pyrolysis waxes under fluid catalytic cracking (FCC) operating conditions. *Waste Manag*, **93**, 162-172.http://www.ncbi.nlm.nih.gov/pubmed/31235053.

Shen, Y., Zhao P, Shao Q, Ma D, Takahashi F, Yoshikawa K. . 2014. In-situ catalytic conversion of tar using rice husk char-supported nickel-iron catalysts for biomass pyrolysis/gasification. *Appl. Catal. B: Environ.*, **152**, 140-151.http://dx.doi.org/10.1016/j.apcatb.2014.01.032.

Sun, S., Li, H, Xu, Z. 2018. Impact of Surface Area in Evaluation of Catalyst Activity. *Joule*, **2**, 1-4.https://doi.org/10.1016/j.joule.2018.05.003.

Sveningsson, M., Morjan R, Nerushev O, Sato Y, Bäckström J, Campbell E, Rohmund F. 2014. Raman spectroscopy and field-emission properties of CVD-grown carbon-nanotube films. *Appl. Phys. A*, **73**(4), 409-418.http://dx.doi.org/10.1007/s003390100923.

Veses, A., Sanahuja-Parejo O, Callen M, Murillo R, Garcia T. 2020. A combined two-stage process of pyrolysis and catalytic cracking of municipal solid waste for the production of syngas and solid refuse-derived fuels. *Waste Manag*, **101**, 171-179.http://www.ncbi.nlm.nih.gov/pubmed/31614284.

Wang, S., Zhao S, Uzoejinwa B, Zheng A, Wang Q, Huang J, Abomohra A. 2020. A state-of-the-art review on dual purpose seaweeds utilization for wastewater treatment and crude bio-oil production. *Energy Convers. Manage.*, **222**, 113253.https://doi.org/10.1016/j.enconman.2020.113253.

Williams, P. 2020. Hydrogen and Carbon Nanotubes from Pyrolysis-Catalysis of Waste Plastics: A Review. *Waste Biomass Valorization*, **12**, 1-28.https://doi.org/10.1007/s12649-020-01054-w.

Wu, C., Williams P. 2009. Investigation of Ni-Al, Ni-Mg-Al and Ni-Cu-Al catalyst for hydrogen production from pyrolysis–gasification of polypropylene. *Appl. Catal. B: Environ.*, **90**(1-2), 147-156.http://dx.doi.org/10.1016/j.apcatb.2009.03.004.

Wu, C., Williams P. 2010. Pyrolysis–gasification of post-consumer municipal solid plastic waste for hydrogen production. *Int. J. Hydrogen Energy*, **35**(3), 949-957.https://pubs.acs.org/doi/10.1016/j.ijhydene.2009.11.045.

Xia, S., Xiao, H., Liu, M., Chen, Y., Yang, H., Chen, H. 2018. Pyrolysis behavior and economics analysis of the biomass pyrolytic polygeneration of forest farming waste. *Bioresour Technol*, **270**,

189-197.https://doi.org/10.1016/j.biortech.2018.09.031.
Xia, S.L.K., Xiao H, Cai N, Dong Z, Xu C, Chen Y, Yang H, Tu X, Chen H. 2019. Pyrolysis of Chinese chestnut shells: Effects of temperature and Fe presence on product composition. *Bioresour Technol*, **287**, 121444.https://doi.org/10.1016/j.biortech.2019.121444.
Xu, L., Lin X, Xi Y, Lu X, Wang C, Liu C. 2014. Alumina-supported Fe catalyst prepared by vapor deposition and its catalytic performance for oxidative dehydrogenation of ethane. *Mater. Res. Bull.*, **59**, 254-260.http://dx.doi.org/10.1016/j.materresbull.2014.07.023.
Xu, S., Cao B, Uzoejinwa B, Odey E, Wang S, Shang H, Li C, Hu Y, Wang Q, Nwakaire J. 2020. Synergistic effects of catalytic co-pyrolysis of macroalgae with waste plastics. *Process Saf. Environ. Prot.*, **137**, 34-48.https://doi.org/10.1016/j.psep.2020.02.001.
Yang, M., Shao J, Yang Z, Yang H, Wang X, Wu Z, Chen H. 2019. Conversion of lignin into light olefins and aromatics over Fe/ZSM-5 catalytic fast pyrolysis: Significance of Fe contents and temperature. *J. Anal. Appl. Pyrolysis*, **137**, 259-265.https://doi.org/10.1016/j.jaap.2018.12.003.
Yang, R., Chuang K, Wey M. 2015. Effects of Nickel Species on Ni/Al2O3 Catalysts in Carbon Nanotube and Hydrogen Production by Waste Plastic Gasification: Bench- and Pilot-Scale Tests. *Energy Fuels*, **29**(12), 8178-8187.https://doi.org/10.1021/acs.energyfuels.5b01866.
Yao, D., Li H, Dai Y, Wang C. 2020a. Impact of temperature on the activity of Fe-Ni catalysts for pyrolysis and decomposition processing of plastic waste. *Chem. Eng. J.*, 127268.https://doi.org/10.1016/j.cej.2020.127268.
Yao, D., Wang C. 2020b. Pyrolysis and in-line catalytic decomposition of polypropylene to carbon nanomaterials and hydrogen over Fe- and Ni-based catalysts. *Appl. Energy*, **265**, 114819.https://doi.org/10.1016/j.apenergy.2020.114819.
Yao, D., Wu C, Yang H, Zhang Y, Nahil M, Chen Y, Williams P. Chen H. 2017. Co-production of hydrogen and carbon nanotubes from catalytic pyrolysis of waste plastics on Ni-Fe bimetallic catalyst. *Energy Convers. Manage.*, **148**, 692-700.http://dx.doi.org/10.1016/j.enconman.2017.06.012.
Yao, D., Zhang Y, Williams P, Yang H, Chen H. 2018. Co-production of hydrogen and carbon nanotubes from real-world waste plastics: Influence of catalyst composition and operational parameters. *Appl. Catal. B: Environ.*, **221**, 584-597.http://dx.doi.org/10.1016/j.apcatb.2017.09.035.
Zhang, Y., Wu C, Nahil M, Williams P. 2015. Pyrolysis–Catalytic Reforming/Gasification of Waste Tires for Production of Carbon Nanotubes and Hydrogen. *Energy Fuels*, **29**(5), 3328-3334.https://doi.org/10.1021/acs.energyfuels.5b00408.
Zhou, L., Guo Y, Hideo K. 2014. Unsupported nickel catalysts for methane catalytic decomposition into pure hydrogen. *AIChE Journal*, **60**(8), 2907-2917.http://dx.doi.org/10.1002/aic.14487.